Selective CO_2 Methanation over Ni Catalysts on Nb-Doped $SrTiO_3$ via Interfacial Electronic Engineering

Haocheng Li[1], Chenwei Wang[1], Yuchen Yan[1], Yiming Li[1], Haotian Li[1], Hongbo Yu[3], Hongfeng Yin*[1, 2]

1 Zhejiang Key Laboratory of Advanced Fuel Cells and Electrolyzers Technology, Ningbo Institute of Materials Technology and Engineering, Chinese Academy of Sciences, Ningbo, Zhejiang, China

2 University of Chinese Academy of Sciences, Beijing, China

3 School of Materials and Chemical Engineering, Ningbo University of Technology, Ningbo, China

Email: yinhf@nimte.ac.cn

Inventory of Supplementary Information

Catalyst Preparation

The $SrTiO_3$ support was synthesized via the hydrothermal method. The detailed steps are as follows: 18 mmol of $Sr(OH)_2 \cdot 8H_2O$ was mixed with 50 ml of 1M acetic acid to yield a transparent solution (A). Subsequently, 18 mmol of $TiCl_4$ was mixed with 20 ml of ethanol to obtain a transparent bright - yellow solution (B). Under a stirring condition, solution B was added to solution A, and 5 g of NaOH was incorporated. The solution gradually increased in viscosity until a gel was formed. The resulting mixture was subjected to a reaction in a 125 mL hydrothermal reactor at 240 °C for 24 h. After cooling, vacuum filtration and washing were carried out. The solid was then placed in an oven at 80 °C for 24 hours for drying.

The preparation method of $SrTi_xNb_{1-x}O_3$ is analogous to that of $SrTiO_3$, merely by substituting $TiCl_4$ with $NbCl_5$ in equivalent proportions.

The Ni/$SrTi_xNb_{1-x}O_3$ catalyst was prepared by the impregnation method. The Ni/$SrTi_xNb_{1-x}O_3$ catalysts with a Ni loading of 3 wt% were prepared by the impregnation method. $Ni(NO_3)_2 \cdot 6H_2O$ was dissolved in deionized water. The $SrTi_xNb_{1-x}O_3$ was added into the mixed solution of precursors under stirring for 12 hours at room temperature, and then rotate to remove the water. The powder obtained dried in a vacuum drying oven at 60 °C overnight, and then calcinated in a muffle furnace at 550 °C for 4 hours at a heating rate of 2 °C·min^{-1}. Before use, the catalyst was reduced in a fixed-bed flow reactor at 500 °C for 2 hours.

Catalytic evaluation

The performance evaluation for CO_2 hydrogenation was performed in a four-channel fixed-bed flow reactor, which used four identical quartz reaction tubes. The catalyst powder was pressed into tablets, and particles of 40-60 mesh were screened out by crushing. 60 mg of catalyst particles were weighed, mixed with 500 mg of 40-60 mesh quartz sand, and then put into a quartz reaction tube. The total flow of H_2, N_2 and CO_2 was controlled by the corresponding mass flow meter (MFC). The flow distribution

system was used to divide the gas flow into four evenly, which were introduced into the four reaction tubes. A three-stage electric heating furnace was used to heat the reaction tube. The catalyst was located in the constant temperature zone of the heating furnace. The exhaust gas passed through a cold trap to condense the water vapor. The selected exhaust gas flowed through the quantitative ring of the electric valve, and then was discharged to the outdoor high altitude. The composition and content of the exhaust gas were analyzed by a Shimadzu GC-2014 chromatographic automatic sample injection analysis. A 60 cm long TDX-01 packed column with an inner diameter of 2 mm was used to separate the components, and the TCD was used as a detector. The detection time was 25 minutes.

Before the reaction, the catalyst was reduced with 30 mL·min^{-1} high-purity H_2 at 650 ºC for 2 hours, and the heating rate was 10 ºC·min^{-1}. After the reduction was complete, cool down to reaction temperature and purge with nitrogen for 10 minutes to desorb the hydrogen adsorbed on the catalyst surface. Then turn off N_2, and pass in mix-gas ($CO_2/H_2/N_2$ = 16/64/20) with 50 mL·min^{-1}. After the reactor was cooled to room temperature, the catalyst was taken out and separated from quartz sand for subsequent analysis and characterization.

The conversion of CH_4, CO_2, and H_2/CO were calculated by the following formula:

The conversion of H_2:

$$C_{H_2} = \frac{F_{H_{2,in}} - F_{H_{2,out}}}{F_{H_{2,in}}} \times 100\%$$

The conversion of CO_2:

$$C_{CO_2} = \frac{F_{CO_{2,in}} - F_{CO_{2,out}}}{F_{CO_{2,in}}} \times 100\%$$

The selectivity of CO:

$$S_{CO} = \frac{F_{CO_{out}}}{F_{CO_{out}} + F_{CH_{4,out}}} \times 100\%$$

The yield of CO:

$$Y_{CO} = C_{CO_2} \times S_{CO} \times 100\%$$

The selectivity of CH_4:

$$S_{CH_4} = \frac{F_{CH_{4,out}}}{F_{CO_{out}} + F_{CH_{4,out}}} \times 100\%$$

The yield of CH_4: $Y_{CH_4} = C_{CO_2} \times S_{CH_4} \times 100\%$ F: Gas flow (mL·min^{-1}),

In: Reactor inlet,

Out: Reactor outlet.

Characterization of materials

X-ray diffraction. The patterns of catalysts were recorded by a Bruker D8 Advance X-ray diffractometer with Cu Kα radiation.

Transmission electron microscopy. The JEOL JEM-F200 field emission electron microscope was used to observe the catalyst microstructure and sample image collection.

Nitrogen adsorption-desorption. Quantachrome Autosorb-3B adsorption instrument was used for nitrogen adsorption-desorption test. The test and analysis methods were as follows: the sample was vacuum-activated at 300 ºC for 3 hours, and then nitrogen was adsorbed and desorbed in a liquid nitrogen bath (77 K) to obtain an isotherm.

X-ray photoelectron spectra. The results were achieved on an AXIS ULTRA DLD multifunctional X-ray photoelectron spectroscope.

H-D exchange experiment. It was carried out on the Tianjin Xianquan TP5080 multi-purpose adsorption apparatus with a MS-GSD 350 OmniStar. 30 mg sample with a particle size of 40-60 mesh was loaded in a quartz tube and pretreated under 30 H_2 mL·min^{-1} at 400 ºC. Then switch the H_2 to 30 mL·min^{-1} Ar to record mass baseline until the H_2 signal dropped to no change on mass spectrometry. After the pre-treatment, the H-D exchange experiment was started and the changes in the signal intensities of the fragments of H_2 (m/z=2), HD (m/z=3) and D_2 (m/z=4) were recorded.

The test for hydrogen spillover. 2 g of WO_3 and 2.0 mg of catalyst were mixed by powder grounding, and 0.5 g of the mixture was placed in a quartz tube and supported with quartz wool. The quartz tube was then positioned in fixed-bed flow reactor. The reactor increased to 105 ºC under N_2 atmosphere, then switched to a mix-gas (H_2:

N_2=1:1, 50 mL/min) and kept it for 5 minutes. WO_3 was used as an indicator to identify the hydrogen spillover on catalysts. The spilled-over hydrogen migrated and readily reacted with the yellow WO_3, resulting in the formation of dark blue H_xWO_3. A darker blue color of WO_3 will indicate a stronger hydrogen spillover.

CO_2 temperature programmed desorption and H_2 temperature programmed reduction. The analyses were acquired using a VDSorb-91i instrument. Prior to CO_2-TPD and H_2-TPR experiments, the samples were pretreated at 100 °C for 60 min in the He flow to remove any adsorbed species.

Temperature programmed surface reaction-mass spectrum. It was carried out on the Tianjin Xianquan TP5080 multi-purpose adsorption apparatus with a GSD 350 OmniStar. The test procedure: 30 mg of a sample with a particle size of 40-60 mesh, and increase the temperature to 400 ºC at a heating rate of 10 ºC·min^{-1} under 30 mL·min^{-1} H_2 purge. Then switch the H_2 to 30 mL·min^{-1} Ar to record mass baseline until the H_2 signal dropped to no change on mass spectrometry. Pulse 1 ml CO_2 into the reactor with 40 mL·min^{-1} Ar, and the the mass spectrum was recorded at the same time. Repeat the above pulse experiment 3-5 times. Then change CO_2 to H_2 with the same pulse experiment. The temperature of reactor was kept at 400 ºC, and the changes in the signal intensities of the fragments of H_2 (m/z=2), CO (m/z=28) and CO_2 (m/z=44) were recorded.

Diffuse reflectance infrared fourier transform spectroscopy. Operando DRIFTS measurements were performed by Vertex 70v Fourier transform infrared spectrometer with a Harrick cell and an MCT detector. The resolution of infrared spectrum collection was 4 cm^{-1}, and the number of collections was 64 times. Before the experiment, the sample was pre-treated in the in-situ cell in an H_2 atmosphere at 650 °C for 1 hour, and then switched to an Ar atmosphere for 30 minutes to eliminate surface adsorbed substances. The background spectrum of the sample was collected under Ar atmosphere. In the first stage, pass H_2 (50 mL·min^{-1}) into the in-situ cell to react for 10 minutes and collect the sample spectrum (30 s/spectrum), and then purge by Ar until there was no gaseous H_2 in the collected sample spectrum. In the second stage, CO_2 (50

mL·min^{-1}) was passed into the in-situ cell for 10 minutes to react and the spectrum of the sample was collected (30 s/spectrum), and then purge by Ar until there was no gaseous CO_2 in the collected sample spectrum. In the third stage, H_2 (50 mL·min^{-1}) was introduced into the in-situ cell for 10 minutes and the sample spectrum was collected (30 s/spectrum). In the fourth stage, the max-gas (CO_2/H_2=1/4, 50 mL·min^{-1}) was passed into the in-situ cell for 10 minutes to react and the spectrum of the sample was collected (30 s/spectrum).

Computational Details

Vienna Ab initio Simulation Package (VASP) software was used to perform all the density functional theory (DFT) calculations[1, 2]. The projector augmented plane wave (PAW) pseudopotential and the Perdew–Burke–Ernzerhof generalized gradient approximation (PBE-GGA) exchange-correlation functional were used to describe the ionic cores[3, 4]. A plane-wave expansion for the basis was set with a cutoff energy of 500 eV. The convergence criterion of total energy was set to be 10-5 eV and that of force on each atom was set to be 0.02 eV/Å.

The model of $SrTiO_3$ (110) slab was modeled by a supercell containing 32 Ti atoms; 32 Sr atoms and 96 O atoms with a vacuum layer of 15 Å to separate the slabs along the perpendicular Z-direction.13 Ti atoms was replaced with Nb atoms to simulate the Nb-doped SrTiO3 (110) slab. A Monkhorst–Pack grid of 2 × 2 × 1 k-points was used for all DFT calculations. To simulate the deposition of Ni on the (110) plane, we constructed Ni10 clusters on the above (110) surface model. First of all, we optimized the two slab structures above. During structural relaxation, the bottom two layers were kept fixed to simulate the bulk anatase. The dissociation and hydrogenation energy barriers of CO2 and CO molecules were estimated using the Nudged Elastic Band (NEB) method.

Supplementary Figures

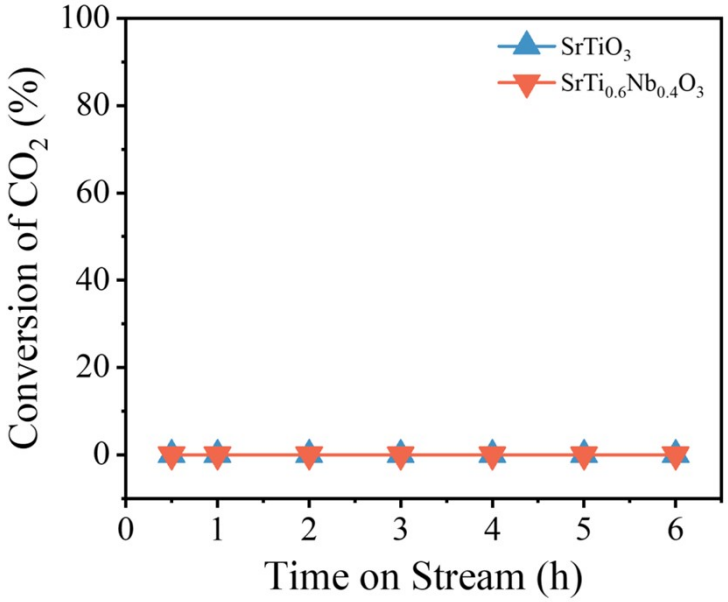

Figure S1 The performance of $SrTiO_3$ and $SrTi_{0.6}Nb_{0.4}O_3$ for CO_2 hydrogenation (Reaction Condition: 400 ℃, H_2/CO=4/1, GWSV=40,000 mL/(g_{cat}·h)).

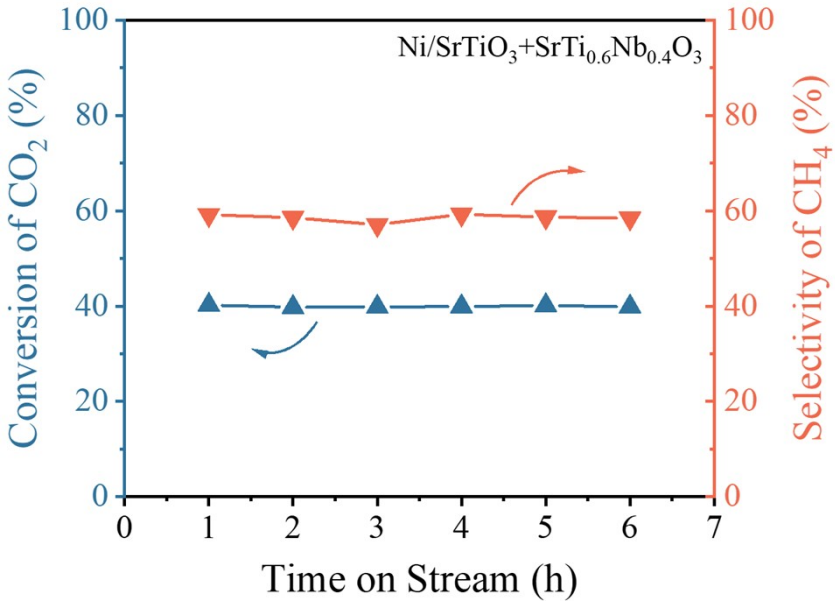

167

168 Figure S2 The catalytic activity of physically mixed catalysts ($Ni/SrTiO_3$ +

169 $SrTi_{0.6}Nb_{0.4}O_3$).

170

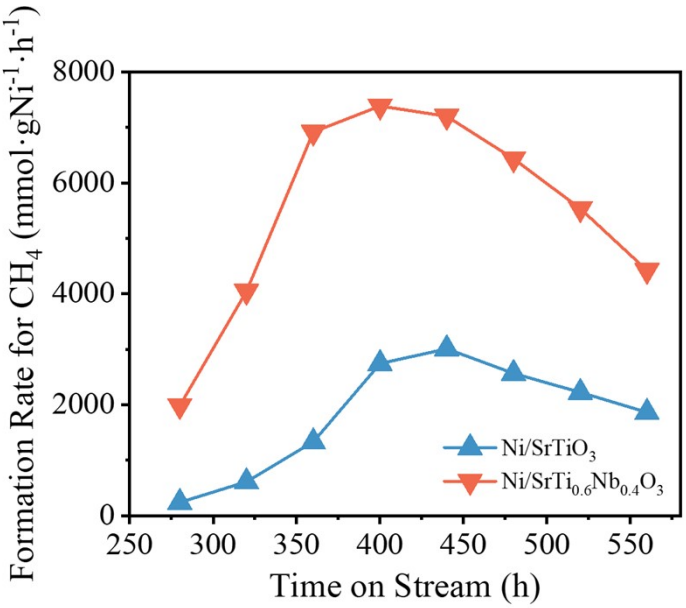

171

172 Figure S3 The formation rate for CH_4 of $Ni/SrTiO_3$ and $Ni/SrTi_{0.6}Nb_{0.4}O_3$ catalysts for

173 CO_2 hydrogenation (Reaction Condition: 280-560 ℃, H_2/CO=4/1, GWSV=40,000

174 mL/(g_{cat}·h)).

175

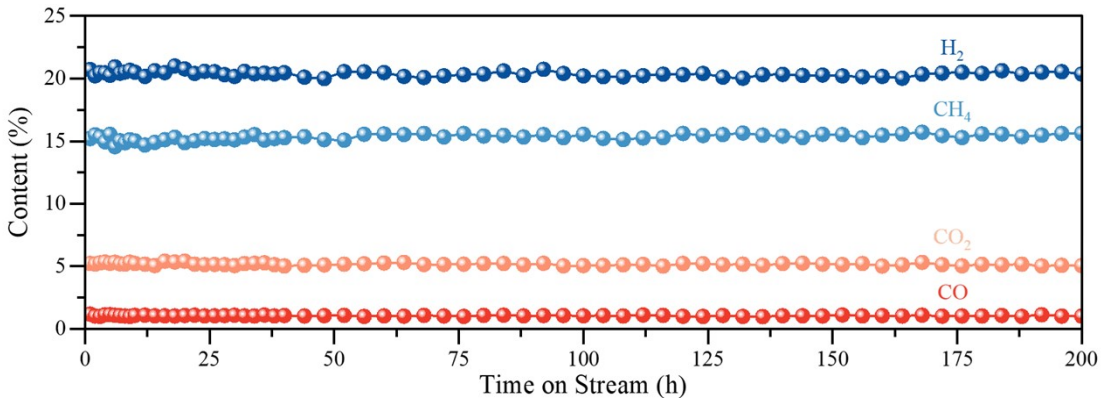

Figure S4 The content during a long-term test of for CO_2 hydrogenation (Reaction Condition: 280-560 °C, H_2/CO=4/1, GWSV=40,000 mL/(g_{cat}·h)).

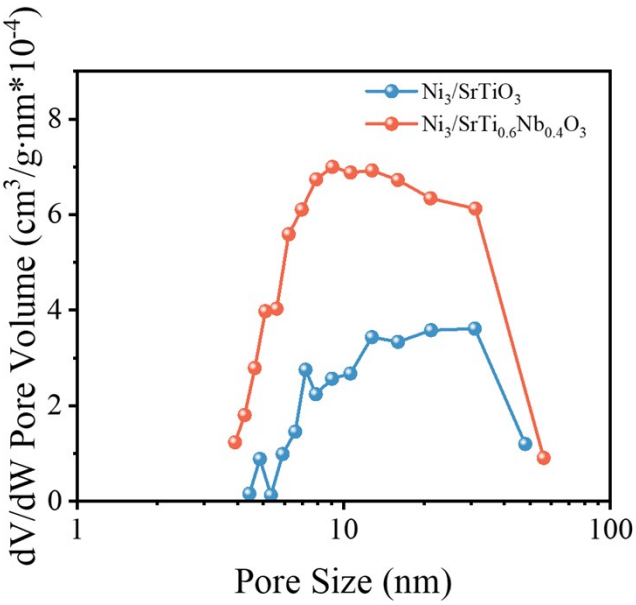

180

181 Figure S5 The pore size distribution plots for $Ni/SrTiO_3$ and $Ni/SrTi_{0.6}Nb_{0.4}O_3$ catalysts.

182

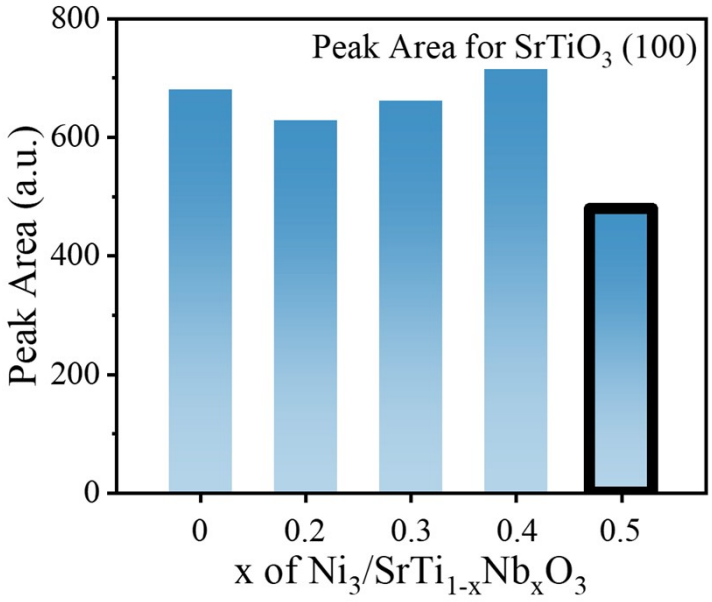

Figure S6 The peak area for $SrTiO_3$ (100) of $Ni/SrTi_{1-x}Nb_xO_3$ catalysts.

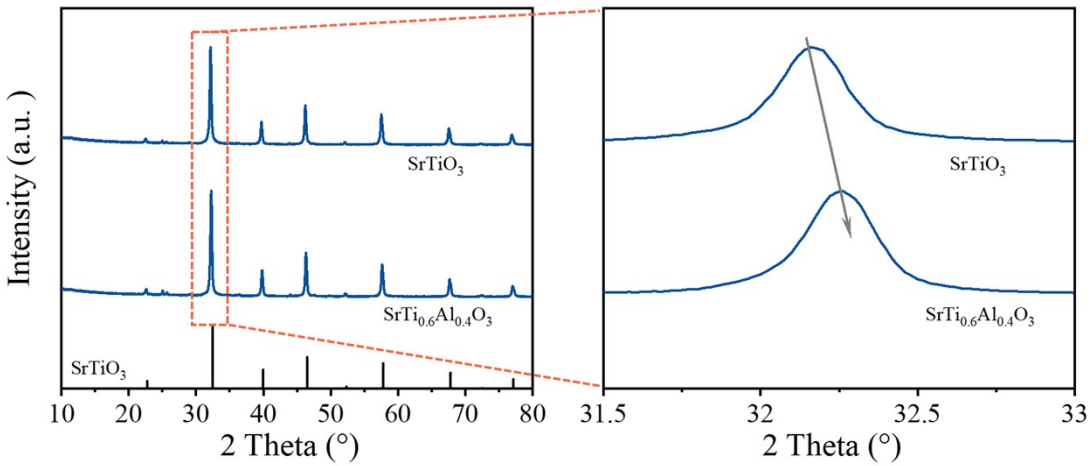

186

187 Figure S7 The XRD patterns for $SrTiO_3$ and $SrTi_{0.6}Al_{0.4}O_3$ catalysts.

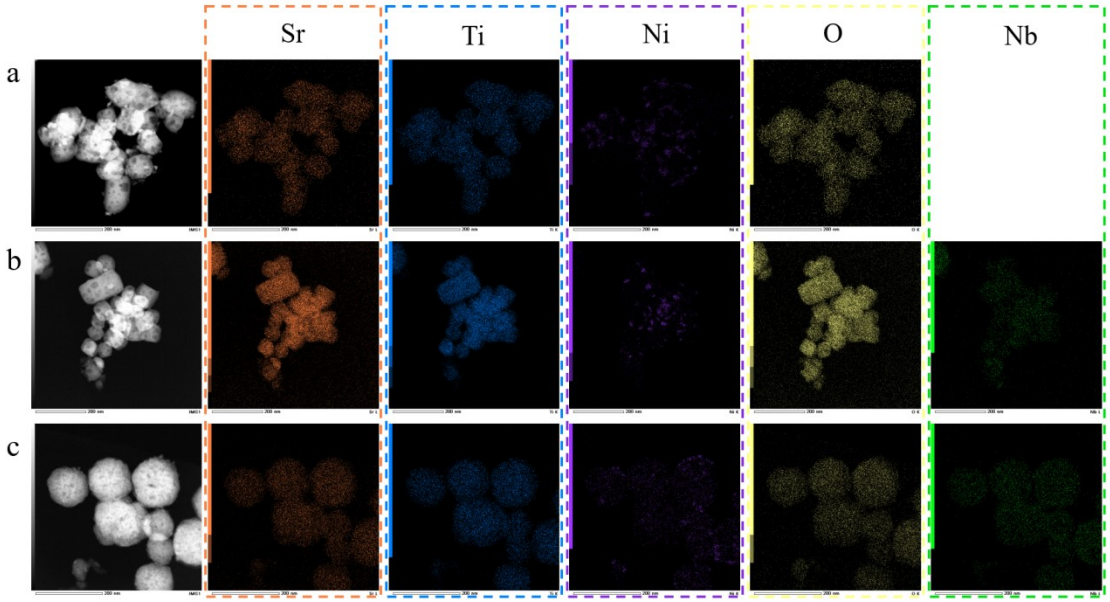

Figure S8 TEM-mapping images for (a) Ni/$SrTiO_3$, (b) Ni/$SrTi_{0.6}Nb_{0.4}O_3$ and (c) Ni/$SrTi_{0.5}Nb_{0.5}O_3$ catalysts.

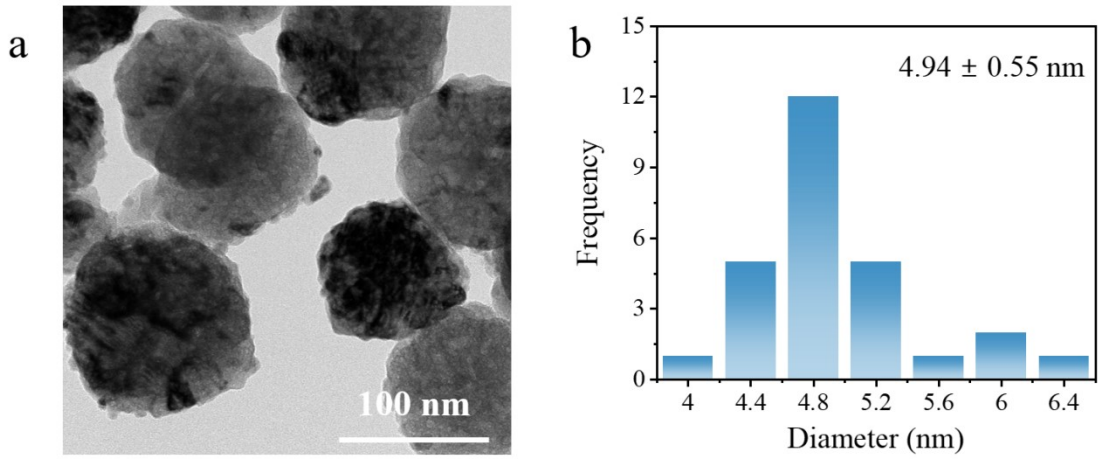

194

195 Figure S9 The (a) TEM image and (b) particle size distribution for $Ni/SrTi_{0.5}Nb_{0.5}O_3$

196 catalyst.

197

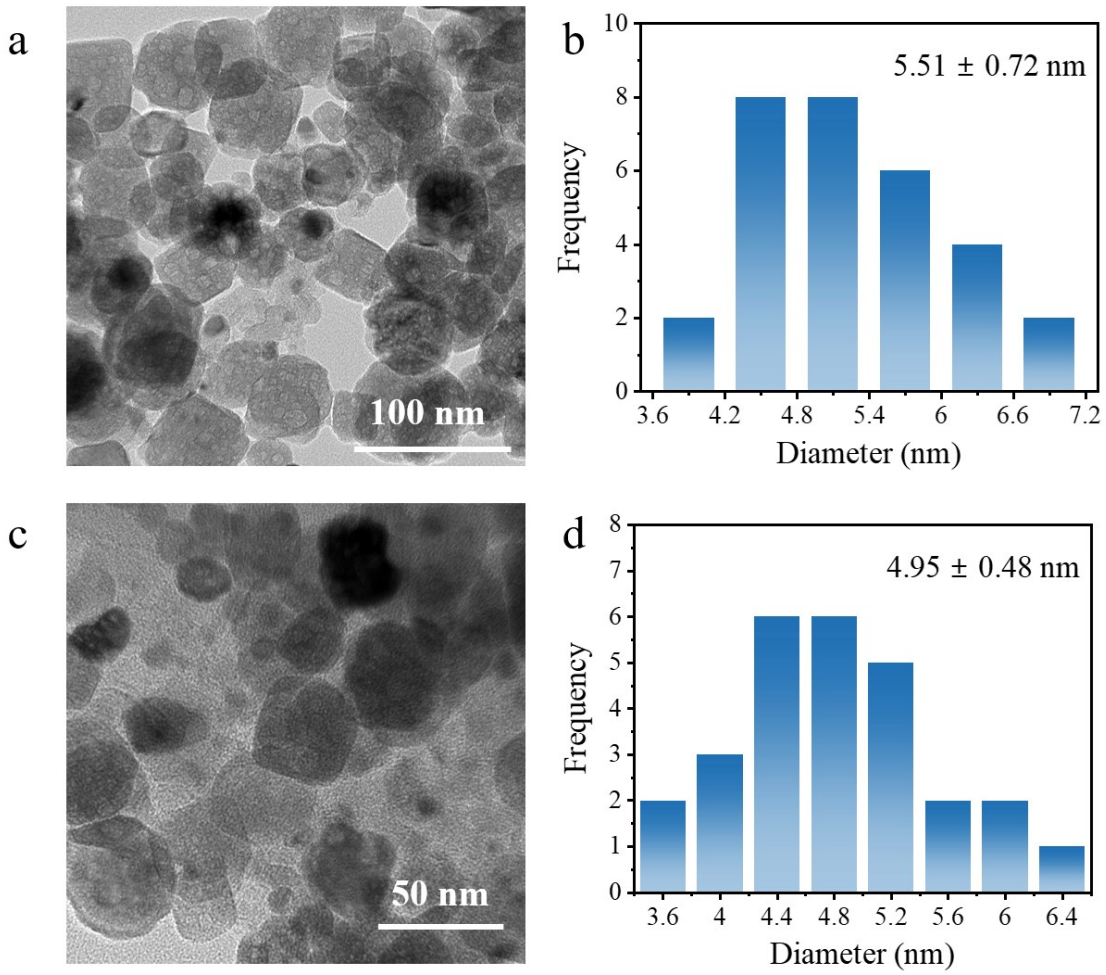

198

199 Figure S10 The TEM image and particle size distribution for (a-b) spent Ni/$SrTiO_3$ and

200 (c-d) spent Ni/$SrTi_{0.6}Nb_{0.4}O_3$ catalysts.

201

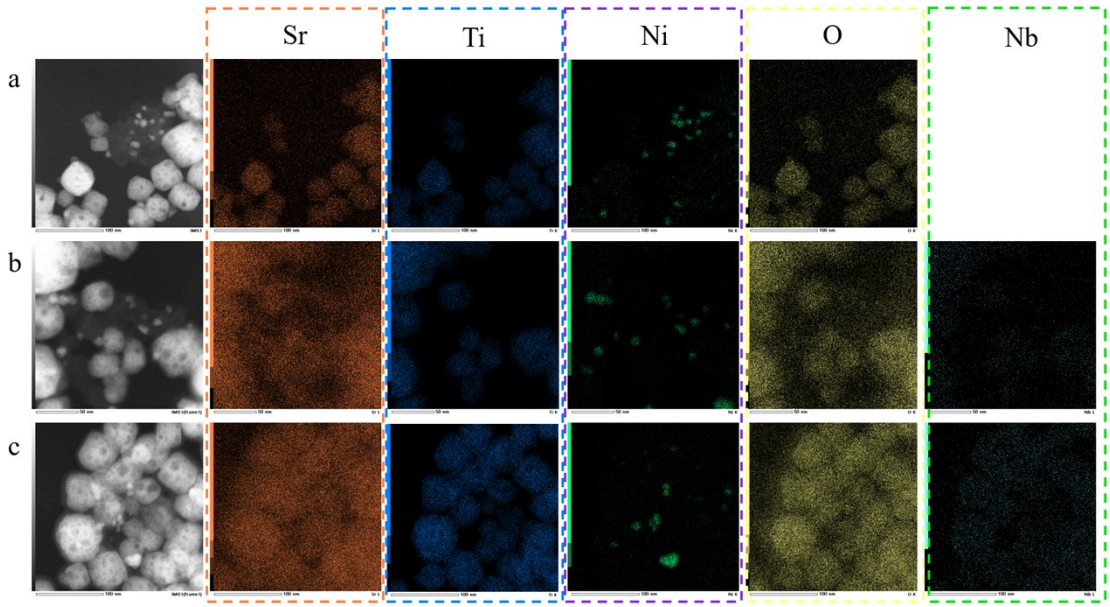

Figure S11 TEM-mapping images for spent catalysts (a) $Ni/SrTiO_3$, (b) $Ni/SrTi_{0.6}Nb_{0.4}O_3$ and (c) $Ni/SrTi_{0.5}Nb_{0.5}O_3$.

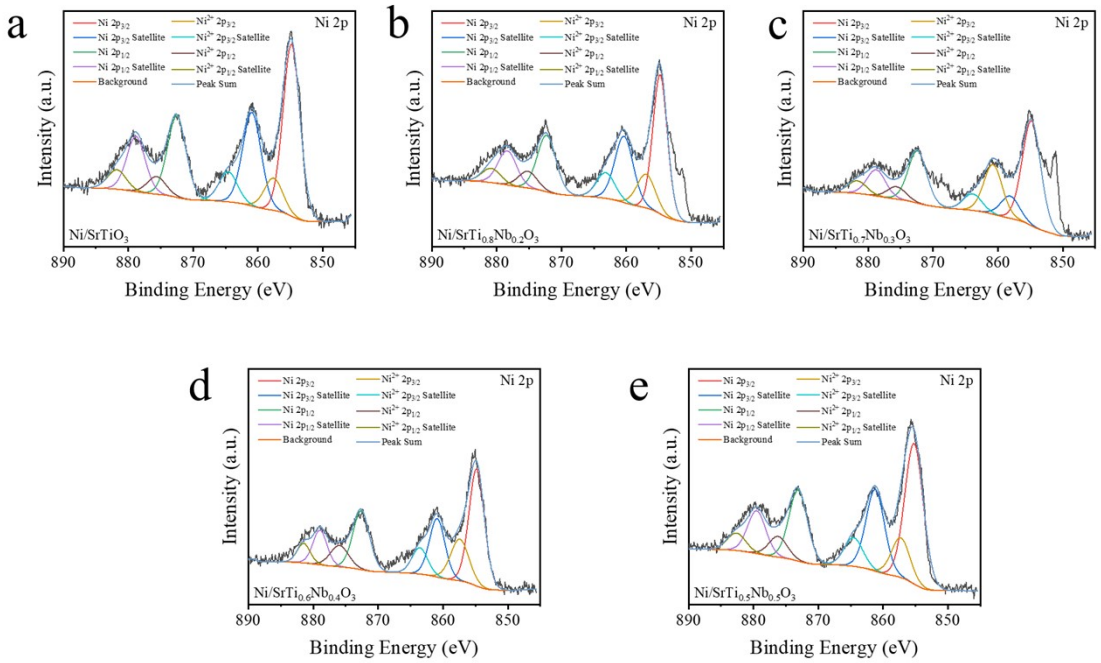

207

208 Figure S12 The XPS spectra of Ni 2p for (a)$Ni/SrTiO_3$, (b) $Ni/SrTi_{0.8}Nb_{0.2}O_3$, (c)

209 $Ni/SrTi_{0.7}Nb_{0.3}O_3$, (d) $Ni/SrTi_{0.6}Nb_{0.4}O_3$, (e) $Ni/SrTi_{0.5}Nb_{0.5}O_3$.

210

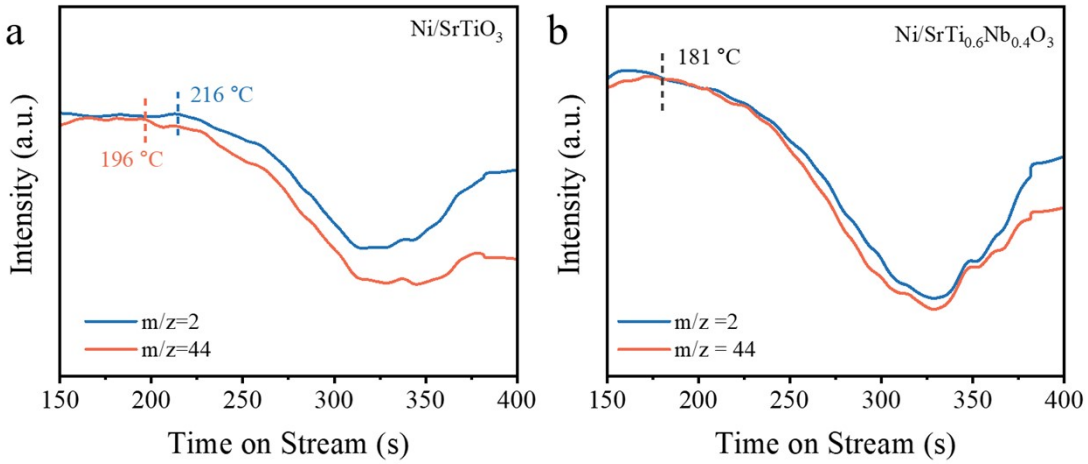

211

212 Figure S13 The differential processed plots of TPSR-MS for (a) $Ni/SrTiO_3$ and (b)

213 $Ni/SrTi_{0.6}Nb_{0.4}O_3$ catalysts.

214

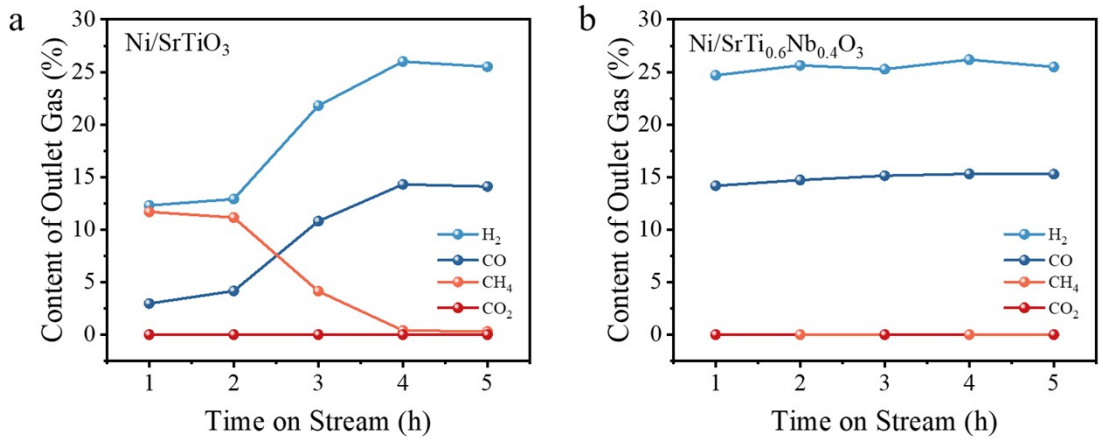

215

216 Figure S14 The performance of $Ni/SrTiO_3$ and $Ni/SrTi_{0.6}Nb_{0.4}O_3$ catalysts for CO

217 hydrogenation (Reaction Condition: 400 °C, $H_2/CO=3/1$, GWSV=32,000 mL/(g_{cat}·h)).

218

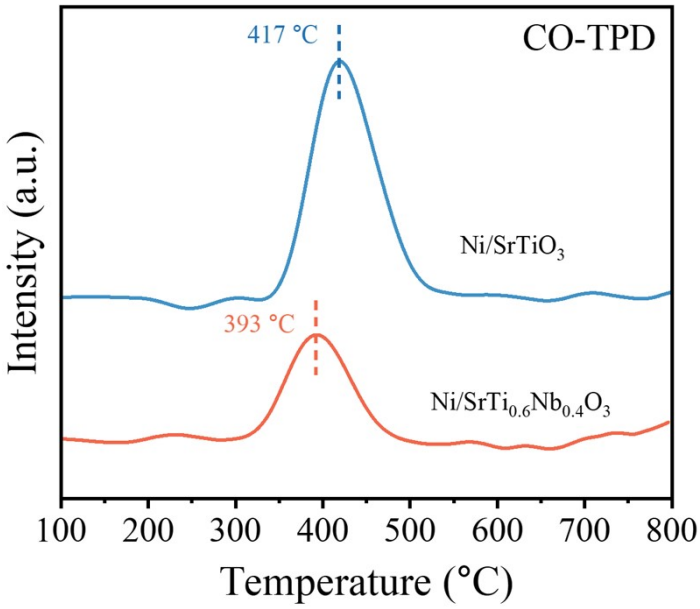

Figure S15 The CO-TPD profiles for $Ni/SrTiO_3$ and $Ni/SrTi_{0.6}Nb_{0.4}O_3$ catalysts.

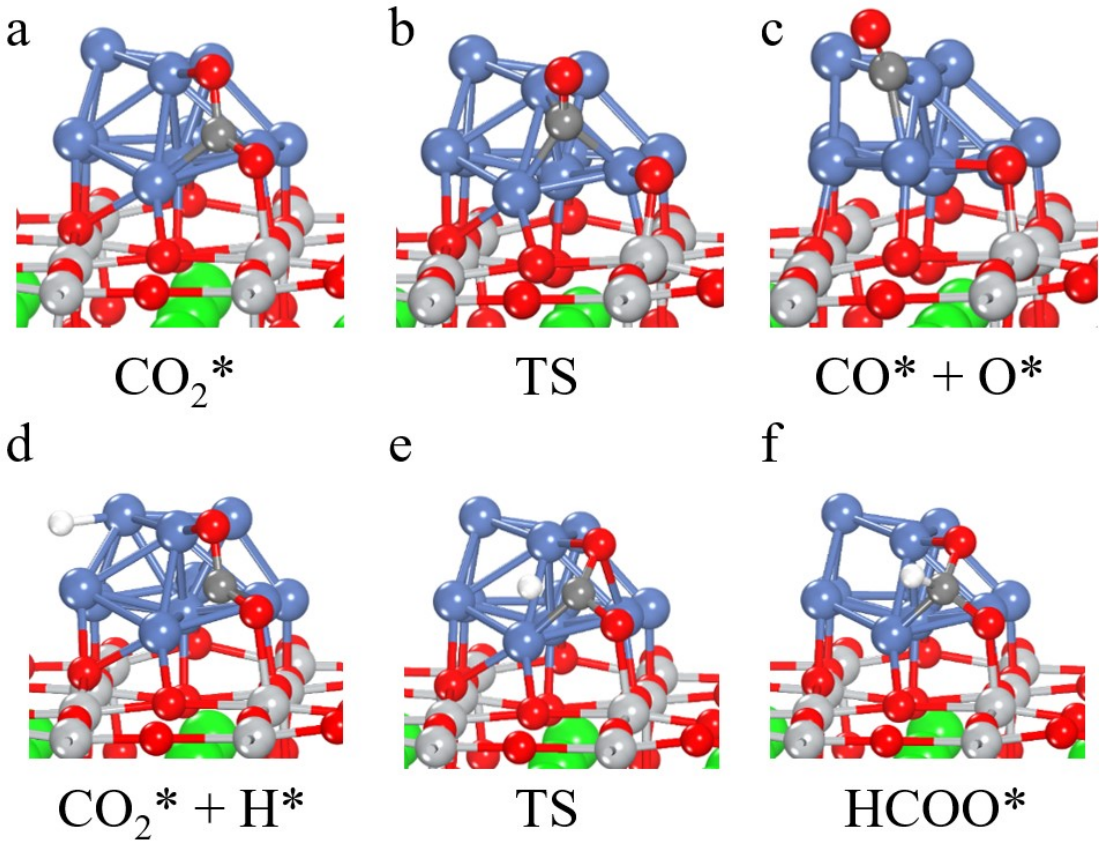

Figure S16 Structure of different CO_2 activation pathway on Ni/$SrTiO_3$ (a-c) CO_2* → CO* + O*, (d-e) CO_2* + H* → HCOO*.

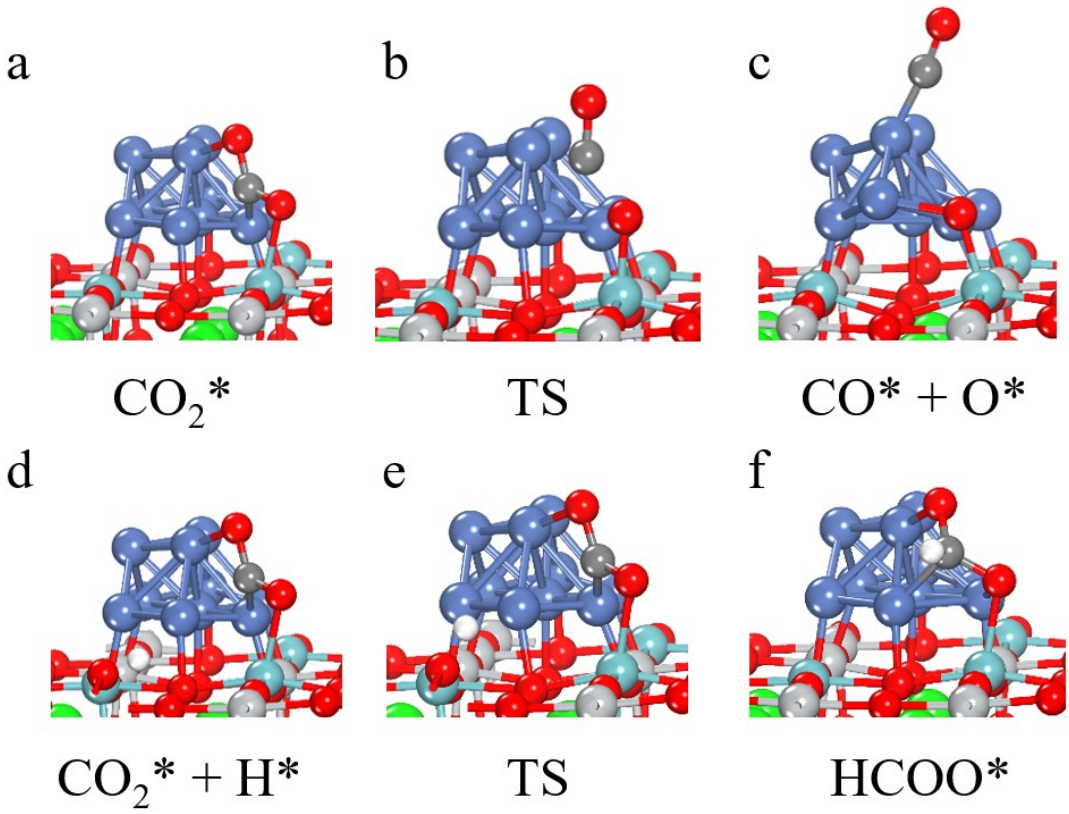

Figure S17 Structure of different CO_2 activation pathway on Ni/$SrTiNbO_3$ (a-c) CO_2* → CO* + O*, (d-e) CO_2* + H* → HCOO*.

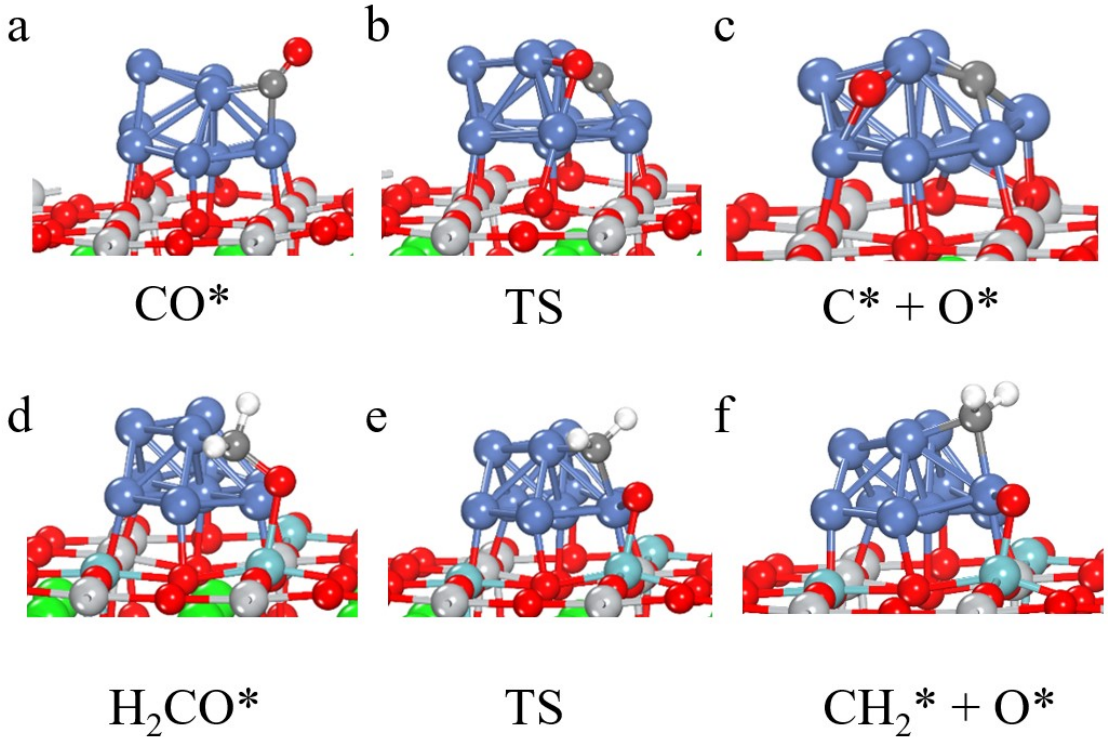

Figure S18 The structure of the rate-determining steps (a-c) CO* → C* + O* on Ni/$SrTiO_3$, (d-e) H_2CO^* → CH_2^* + O* on Ni/$SrTiNbO_3$.

Supplementary Tables

Sample	Peak Intensity of Ni^0	Peak Intensity of Ni^{2+}	Content of O_v
$Ni/SrTiO_3$	40983	28739	58.8 %
$Ni/SrTi_{0.8}Nb_{0.2}O_3$	33481	20444	62.1 %
$Ni/SrTi_{0.7}Nb_{0.3}O_3$	32372	15333	67.9 %
$Ni/SrTi_{0.6}Nb_{0.4}O_3$	30114	13080	69.7 %
$Ni/SrTi_{0.5}Nb_{0.5}O_3$	45892	29118	61.2 %

Table S1 XPS Ni 2p analysis of $Ni/SrTi_xNb_{1-x}O_3$.

237 Table S2 Bader charge analysis of $Ni/SrTiO_3$ and $Ni/SrTiNbO_3$.

$Ni/SrTiO_3$			$Ni/SrTiNbO_3$		
Atom name	Bader	Δe	Atom name	Bader	Δe
Ni1	9.78	-0.22	Ni1	10.02	0.02
Ni2	9.91	-0.09	Ni2	10.00	0.00
Ni3	9.88	-0.12	Ni3	10.00	0.00
Ni4	9.79	-0.21	Ni4	10.02	0.02
Ni5	9.88	-0.12	Ni5	9.97	-0.03
Ni6	9.86	-0.14	Ni6	9.99	-0.01
Ni7	9.80	-0.20	Ni7	9.93	-0.07
Ni8	10.09	-0.09	Ni8	10.14	0.14
Ni9	10.03	0.03	Ni9	10.12	0.12
Ni10	10.20	0.20	Ni10	10.16	0.16
Average		-0.08	Average		0.03

238

239 Table S3 XPS O 1s analysis of $Ni/SrTi_xNb_{1-x}O_3$.

Sample	Peak Intensity of O_l	Peak Intensity of O_v	Peak Intensity of O_c	Content of O_v
$Ni/SrTiO_3$	12681	6128	4121	26.7 %
$Ni/SrTi_{0.8}Nb_{0.2}O_3$	18554	10651	4821	31.3 %
$Ni/SrTi_{0.7}Nb_{0.3}O_3$	9601	7716	4867	34.8 %
$Ni/SrTi_{0.6}Nb_{0.4}O_3$	10076	10695	3170	44.7 %
$Ni/SrTi_{0.5}Nb_{0.5}O_3$	15425	10863	3796	36.1 %

240

241

242

Table S4 The calculated energy of intermediate compounds in CO_2 activation processes on Ni/$SrTiO_3$(110) and Ni/$SrTiNbO_3$(110).

Ni/$SrTiO_3$(110)		Ni/$SrTiNbO_3$(110)	
CO_2*	-1316.69	CO_2*	-1330.55
TS	-1316.16	TS	-1329.91
CO* + O*	-1316.98	CO* + O*	-1331.29
$\triangle E_1$	0.53	$\triangle E_1$	0.64
CO_2* + H*	-1320.72	CO_2* + H*	-1333.27
TS	-1319.44	TS	-1332.71
HCOO*	-1319.72	HCOO*	-1334.01
$\triangle E_2$	1.28	$\triangle E_2$	0.56

Table S5 The calculated energy of intermediate compounds in rate-determining steps on $Ni/SrTiO_3(110)$ and $Ni/SrTiNbO_3(110)$.

$Ni/SrTiO_3(110)$		$Ni/SrTiNbO_3(110)$	
CO*	-1309.24	H_2CO*	-1329.97
TS	-1307.22	TS	-1329.59
C* + O*	-1310.03	CH_2* + O*	-1331.01
$\triangle E_3$	1.82	$\triangle E_3$	0.38

Supplementary Reference

(1) Kresse, G.; Furthmu¨ller, J. Efficient iterative schemes for ab initio total-energy calculations using a plane-wave basis set. *Physical Review B* **1996**, *54*, 11169-11186.

(2) Kresse, G.; Joubert, D. From ultrasoft pseudopotentials to the projector augmented-wave method. *Physical Review B* **1999**, *59*, 1758-1775.

(3) Perdew, J. P.; Burke, K.; Ernzerhof, M. Generalized Gradient Approximation Made Simple. *Physical Review Letters* **1996**, *77*, 3865-3868.

(4) Blöchl, P. E. Projector augmented-wave method. *Physical Review B* **1994**, *50* (24), 17953-17979. DOI: 10.1103/PhysRevB.50.17953.